

HELIUM NOVA ON A VERY MASSIVE WHITE DWARF: A REVISED LIGHT-CURVE MODEL OF V445 PUPPIS (2000)

MARIKO KATO

Department of Astronomy, Keio University, Hiyoshi, Kouhoku-ku, Yokohama 223-8521, Japan; mariko@educ.cc.keio.ac.jp

IZUMI HACHISU

Department of Earth Science and Astronomy, College of Arts and Sciences, University of Tokyo, Komaba, Meguro-ku,
Tokyo 153-8902, Japan; hachisu@ea.c.u-tokyo.ac.jp

SEIICHIRO KIYOTA

4-405-1003 Matsushiro, Tsukuba 305-0035, Japan; skiyota@nias.affrc.go.jp

AND

HIDEYUKI SAIO

Astronomical Institute, Graduate School of Science, Tohoku University, Sendai 980-8578, Japan; saio@astr.tohoku.ac.jp

Received 2007 December 29; accepted 2008 May 15

ABSTRACT

V445 Pup (2000) is a unique object identified as a helium nova. Color indexes during the outburst are consistent with those of free-free emission. We present a free-free emission–dominated light-curve model of V445 Pup on the basis of the optically thick wind theory. Our light-curve fitting shows that (1) the white dwarf (WD) mass is very massive ($M_{\text{WD}} \gtrsim 1.35 M_{\odot}$) and (2) half of the accreted matter remains on the WD, both of which suggest that the WD mass is increasing. Therefore, V445 Pup is a strong candidate for a Type Ia supernova progenitor. The estimated distance to V445 Pup is now consistent with recent observational suggestions, $3.5 \text{ kpc} \lesssim d \lesssim 6.5 \text{ kpc}$. A helium star companion is consistent with the brightness of $m_v = 14.5 \text{ mag}$ just before the outburst, if it is a slightly evolved hot ($\log T[\text{K}] \gtrsim 4.5$) star with the mass of $M_{\text{He}} \gtrsim 0.8 M_{\odot}$. We then emphasize importance of observations in the near-future quiescent phase after the thick circumstellar dust dissipates away, especially its color and magnitude, to specify the nature of the companion star. We have also calculated helium ignition masses for helium shell flashes against various helium accretion rates and discussed the recurrence period of helium novae.

Subject headings: binaries: close — novae, cataclysmic variables — stars: individual (V445 Puppis) — stars: mass loss — white dwarfs

Online material: color figures

1. INTRODUCTION

The outburst of V445 Pup was discovered on 2000 December 30 by Kanatsu (Kato et al. 2000). The outburst shows unique properties such as the absence of hydrogen and unusually strong carbon emission lines, as well as strong emission lines of Na, Fe, Ti, Cr, Si, Mg, etc. (Ashok & Banerjee 2003; Iijima & Nakanishi 2008). The spectral features resemble those of classical slow novae, except for the absence of hydrogen and strong emission lines of carbon (Iijima & Nakanishi 2008). The development of the light curve is very slow (3.3 mag decline in 7.7 months), with a small outburst amplitude of 6 mag. From these features, it has been suggested that this object is the first example of a helium nova (Ashok & Banerjee 2003; Kato & Hachisu 2003).

In our earlier work (Kato & Hachisu 2003), we presented a theoretical light-curve model with the assumption of blackbody emission from the photosphere, which resulted in the best-fit model of a very massive white dwarf (WD; $M_{\text{WD}} \gtrsim 1.3 M_{\odot}$) and a relatively short distance of $d \lesssim 1 \text{ kpc}$. However, Iijima & Nakanishi (2008) recently showed that there are absorption lines of the Na I D doublet at the velocities of 16.0 and 73.5 km s⁻¹, suggesting that V445 Pup is located in or beyond the Orion arm and that its distance is as large as 3.5–6.5 kpc. Woudt & Steeghs (2005) also suggested a large distance of 4.9 kpc. Moreover, color indexes during the outburst are consistent with those of free-free emission. With these new observational aspects, we have revised the light-curve model of V445 Pup.

Helium novae were theoretically predicted by Kato et al. (1989) as a nova outburst caused by a helium shell flash on a white dwarf. Such helium novae have long been theoretical objects until the first helium nova, V445 Pup, was discovered in 2000. Kato et al. (1989) assumed two types of helium accretion: helium accretion from a helium star companion and hydrogen-rich matter accretion at a high accretion rate with, beneath the steady hydrogen-burning shell, ash helium accumulating on the WD. The latter case is divided into two kinds of systems, depending on whether hydrogen shell burning is steady (stable) or not. To summarize, helium accretion onto a WD occurs in three types of systems: (1) helium accretion from a helium star companion; (2) steady hydrogen accretion with a rate high enough to keep steady hydrogen shell burning, such as supersoft X-ray sources, e.g., RX J0513.9–6951 (e.g., Hachisu & Kato 2003; McGowan et al. 2005) and CAL 83 (e.g., Schmidtke & Cowley 2006); and (3) hydrogen accretion at a relatively low rate, resulting in a recurrent nova such as RS Oph (e.g., Hachisu et al. 2007) and U Sco (e.g., Hachisu et al. 2000). In the present paper, we regard V445 Pup as case (1), because no hydrogen lines were detected (Iijima & Nakanishi 2008).

In helium novae, mass loss because of an optically thick wind is relatively weak compared to hydrogen novae, and a large part of the accreted helium burns into carbon and oxygen and accumulates on the WD (Kato & Hachisu 1999; Kato & Hachisu 2004). Our previous model indicated that V445 Pup contains a massive WD ($M_{\text{WD}} \gtrsim 1.3 M_{\odot}$), and the WD mass is increasing

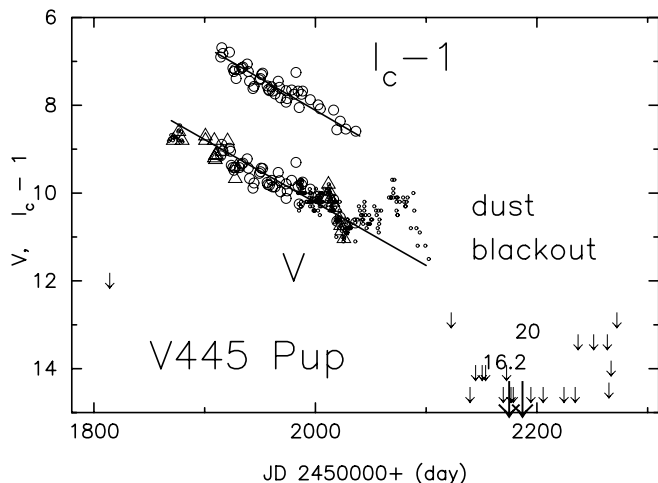


FIG. 1.— V and I_C light curves of V445 Pup (large open circles). The I_C data are shifted up by 1 mag in order to separate it from the V light curve. Open triangles denote V magnitudes (Kato et al. 2000; IAU Circs. 7553, 7557, 7559, 7569, and 7620). Small open circles and downward arrows are taken from AAVSO to show very early and later phases of the outburst. Large downward arrows show an upper limit observation of $I_C > 16.2$ (this work), $V > 20$ and $I > 19.5$ (at the same date; Henden et al. 2001). Straight lines indicate the average decline rates of $1.9 \text{ mag}/130 \text{ days} = 0.0146 \text{ mag day}^{-1}$ and $3.3 \text{ mag}/230 \text{ days} = 0.0143 \text{ mag day}^{-1}$ for I_C and V , respectively. [See the electronic edition of the Journal for a color version of this figure.]

through helium shell flashes. Therefore, V445 Pup is a strong candidate for a Type Ia supernova progenitor. Although there are two known evolutionary paths of the single-degenerate scenario toward Type Ia supernovae (e.g., Hachisu et al. 1999), helium-accreting WDs such as V445 Pup do not belong to either of them. Therefore, it may indicate the third path to Type Ia supernovae. If various binary parameters of V445 Pup are determined, they can provide us with important clues to binary evolution toward Type Ia supernovae.

In § 2 we introduce our multiband photometric observations, which indicates that free-free emission dominates in the optical and near-infrared. In § 3 we present our free-free emission-dominated light-curve model and its application to V445 Pup. Then we discuss brightness in quiescence in § 4. Discussion and conclusions follow in §§ 5 and 6, respectively.

2. OBSERVATIONS

Shortly after the discovery of the V445 Pup outburst, one of us (S. K.) started multiband photometry with a 25.4 cm telescope [focal length 1600 mm, CCD camera Apogee AP-7 (SITE SIA502AB of 512×512 pixels)]. V and R_C magnitudes are obtained from 2001 January 4 to May 6 and I_C from 2001 January 4 to 2007 January 15, with the comparison star, TYC 6543-2917-1 ($V = 8.74$, $B - V = 0.304$). All of our data can be found at the data archive of the Variable Star Observers League in Japan (VSOLJ).¹

Figure 1 shows our V and I_C magnitudes, as well as other observations taken from the literature. These two light curves show very slow evolution ($\sim 0.014 \text{ mag day}^{-1}$), followed by an oscillatory behavior in the V magnitude before it quickly darkened because of a dust blackout on about JD 2,452,100, i.e., 7.5 months after the discovery (Henden et al. 2001; Woudt 2002; Ashok & Banerjee 2003). Here we assume the decline rate of the light curves as shown in Figure 1, ignoring the later oscillatory phase (JD 2,452,040–2,452,100), because we assume a steady state in the nova envelope, as mentioned below,

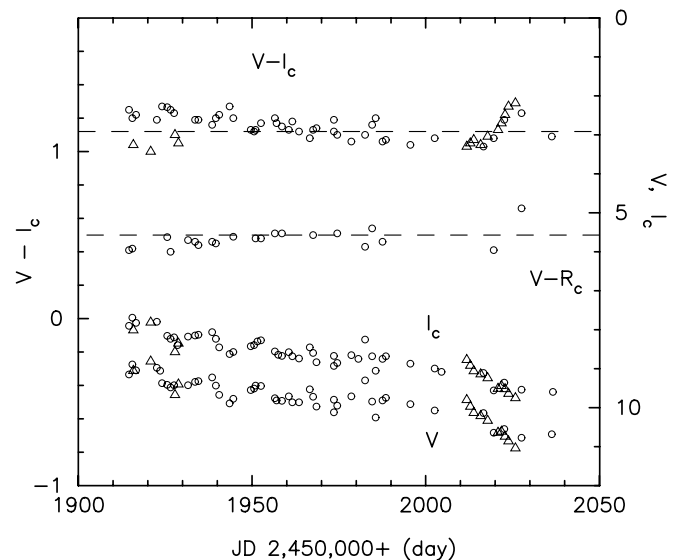


FIG. 2.— Color indexes of $V - I_C$ and $V - R_C$, as well as I_C and V . Circles, this work; triangles, Gilmore (IAU Circs. 7559 and 7569) and Gilmore & Kilmartin (IAU Circ. 7620). The horizontal dashed lines indicate the mean values of $V - R_C = 0.5$ and $V - I_C = 1.12$.

and as a result, our theoretical light curve cannot treat unsteady oscillations.

Figure 2 shows the evolution of color indexes $V - I_C$ and $V - R_C$, as well as V and I_C themselves. We can see that both of $V - I_C$ and $V - R_C$ are almost constant with time, i.e., ≈ 1.12 and ≈ 0.5 , respectively, during our observation. This means that the three light curves of V , I_C , and R_C are almost parallel, and each light-curve shape is independent of wavelength. These are the characteristic properties of free-free emission-dominated light curves, as explained below.

The flux of optically thin free-free emission is inversely proportional to the square of the wavelength, i.e., $F_\lambda \propto \lambda^{-2}$. This spectrum shape is unchanged with time, although the electron temperature rises during nova outburst because the emission coefficient depends only very slightly on the electron temperature (e.g., Brown & Mathews 1970). Therefore, the color indexes of free-free emission-dominated light curves are unchanged with time. On the other hand, the color indexes change with time if blackbody emission dominates, because the photospheric temperature rises with time in nova outbursts. Figures 1 and 2 indicate that the emission from V445 Pup is dominated by free-free emission, rather than by blackbody emission.

The color index of free-free emission is calculated from $\lambda F_\lambda \propto \lambda^{-1}$. When the reddening is known, the reddened color is obtained as

$$m_V - m_\lambda = (M_V - M_\lambda)_0 + c_\lambda E(B - V), \quad (1)$$

where $(M_V - M_\lambda)_0$ is the intrinsic color and c_λ is the reddening coefficient (these values are tabulated in Table 4 in Hachisu et al. [2008] for five colors of $V - R$, $V - I$, $V - J$, $V - H$, and $V - K$). Figure 3 shows the color indexes relative to V for two cases of reddening, i.e., $E(B - V) = 0$ and 0.5 .

For comparison, we have added four relative colors of V1500 Cyg (Hachisu & Kato 2006), because its continuum flux is known to be that of free-free emission (Gallagher & Ney 1976), except for the first few days after the optical peak. Here we use Strömgren y -magnitude instead of V , because the intermediate-width y band is almost emission line-free. Three ($y - I$, $y - H$, and $y - K$) of

¹ See <http://vsolj.cetus-net.org>.

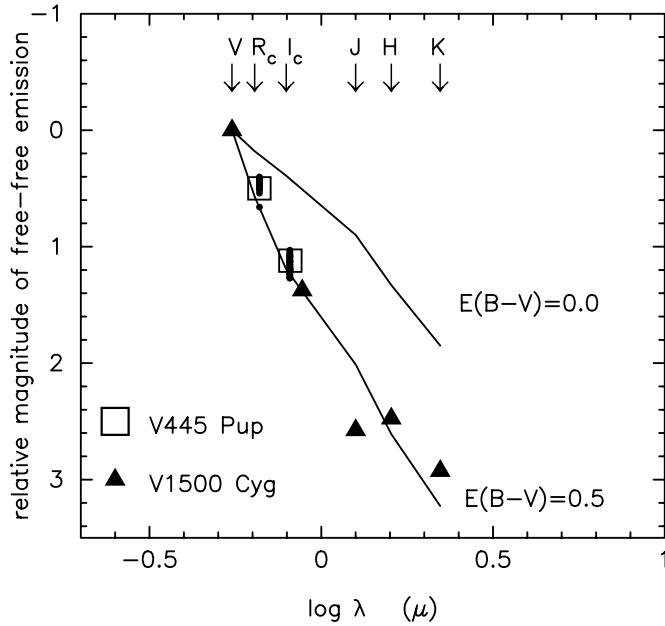


FIG. 3.—Color indexes plotted against wavelength. Our observational color indexes of V445 Pup, $V - R_c$ and $V - I_c$, are plotted for individual data (dots) and their mean values of 0.5 and 1.12 (squares). The color indexes of V1500 Cyg are added for y -magnitude instead of V (triangles; taken from Hachisu et al. 2008). Arrows indicate the effective wavelength of six bands, V , R_c , I_c , J , H , and K . Curves denote color indexes of free-free emission for $E(B - V) = 0$ and 0.5. [See the electronic edition of the Journal for a color version of this figure.]

four color indexes are consistent with those of color indexes with $E(B - V) = 0.5$ (Ferland 1977; Hachisu & Kato 2006). The J band is strongly contaminated with strong emission lines of He I (e.g., Black & Gallagher 1976; Kolotilov & Liberman 1976; Shenavrin & Moroz 1976). This is the reason the $y - J$ color index deviates from that of free-free emission (see Hachisu et al. 2008 for more details).

Our observed color indexes are shown in Figure 3. The squares are centered at the mean values of $V - R_c = 0.5$ and $V - I_c = 1.12$, whereas dots represent individual observations. In V445 Pup, no strong emission lines dominate the continuum in the V , R , and I bands (Kamath & Anupama 2002; Iijima & Nakanishi 2008). Therefore, we conclude that the color indexes of V445 Pup are consistent with those of free-free emission with the reddening of $E(B - V) = 0.51$ (Iijima & Nakanishi 2008).

3. MODELING OF NOVA LIGHT CURVES

3.1. Basic Model

After a thermonuclear runaway sets in on the surface of a WD, the envelope expands to giant size and the optical luminosity reaches its maximum. Optically thick winds occur, and the envelope reaches a steady state. Using the same method and numerical techniques as in Kato & Hachisu (1994, 2003), we have followed the evolution of a nova by connecting steady state solutions along the sequence of decreasing envelope mass. We have solved the equations of motion, continuity, radiative diffusion, and conservation of energy from the bottom of the helium envelope through the photosphere. The winds are accelerated deep inside the photosphere. Updated OPAL opacities are used (Iglesias & Rogers 1996). As one of the boundary conditions for our numerical code, we assume that photons are emitted at the photosphere as a blackbody with a photospheric temperature T_{ph} . Kato & Hachisu (2003) calculated the visual magnitude M_V on the basis of blackbody emission and constructed the light curves.

TABLE 1
MODEL PARAMETERS

M_{WD} (M_{\odot})	$\log R_{\text{WD}}$ (R_{\odot})	Y	$X_{\text{C+O}}$
1.2.....	-2.193	0.68	0.3
1.3.....	-2.33	0.48	0.5
1.33.....	-2.417	0.38	0.6
1.35.....	-2.468	0.38	0.6
1.37.....	-2.535	0.58	0.4
1.37.....	-2.535	0.38	0.6
1.37.....	-2.535	0.18	0.8
1.377.....	-2.56	0.38	0.6

NOTE.—The heavy-element content is assumed to be $Z = 0.02$, which includes carbon and oxygen in the solar ratio.

In the present work, we calculate free-free emission-dominated light curves. The envelope structure, wind mass-loss rate, photospheric temperature, and photospheric radius of the WD envelope are essentially the same as those in the previous model.

The flux of free-free emission from the optically thin region outside the photosphere dominates in the continuum flux of optical and near-infrared wavelength region and is approximated by

$$F_{\nu} \propto \int N_e N_i dV \propto \int_{R_{\text{ph}}}^{\infty} \frac{\dot{M}_{\text{wind}}^2}{v_{\text{wind}}^2 r^4} r^2 dr \propto \frac{\dot{M}_{\text{wind}}^2}{v_{\text{ph}}^2 R_{\text{ph}}}, \quad (2)$$

where F_{ν} is the flux at the frequency ν , N_e and N_i are the number densities of electrons and ions, respectively, V is the volume, R_{ph} is the photospheric radius, \dot{M}_{wind} is the wind mass-loss rate, and v_{ph} is the photospheric velocity (Hachisu & Kato 2006; Hachisu et al. 2008).

The proportionality constant in equation (2) cannot be determined a priori because we do not calculate radiative transfer outside the photosphere. These proportionality constants are determined by fitting with observational data (Hachisu & Kato 2006, 2007; Hachisu et al. 2008).

3.2. Free-Free Light Curve and WD Mass

We have calculated free-free emission-dominated light curves of V445 Pup for WD masses of 1.2, 1.3, 1.33, 1.35, 1.37, and 1.377 M_{\odot} . The last one is the upper limit of the mass-accreting WDs (Nomoto et al. 1984). The adopted WD radius and chemical composition are listed in Table 1. Here we assume that chemical composition is constant throughout the envelope.

Figure 4 shows the calculated free-free light curves. More massive WDs show faster declines. This is mainly because more massive WDs have less massive envelopes, and the smaller mass envelopes are quickly taken off by the wind. The figure also shows two additional models of $M_{\text{WD}} = 1.37 M_{\odot}$ with different compositions of $X_{\text{C+O}} = 0.4$ and 0.8. These models show decline rates almost similar to that of $M_{\text{WD}} = 1.37 M_{\odot}$ with $X_{\text{C+O}} = 0.6$.

The starting point of our model light curve depends on the initial envelope mass. When an initial envelope mass is given, our nova model is located somewhere on the light curve. For a more massive ignition mass, it starts from an upper point of the light curve. Then the nova moves rightward with the decreasing envelope mass due to wind mass loss and nuclear burning.

Helium shell flashes develop much more slowly than hydrogen shell flashes, mainly because of the much larger envelope masses of helium shell flashes (Kato & Hachisu 1994). The short straight solid line in Figure 4 represents the decline rate of the

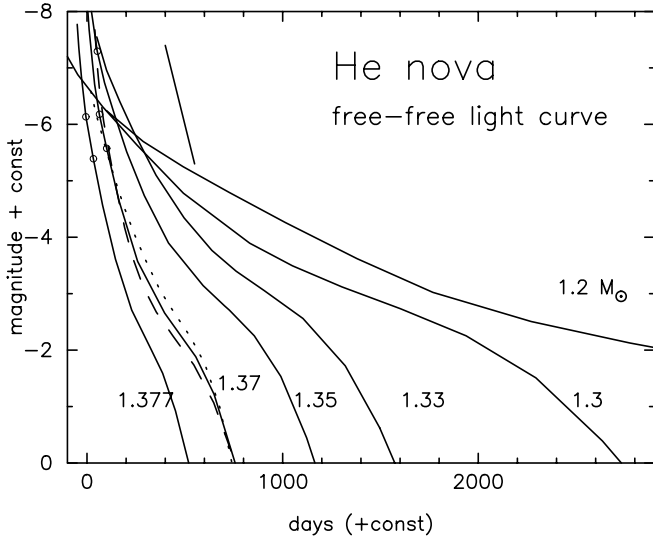


FIG. 4.—Free-free emission-dominated light curves for various WD masses. The chemical composition is assumed to be $Y = 0.38$, $X_{C+O} = 0.6$, and $Z = 0.02$ throughout the envelope. The WD mass is shown for each curve. The dashed and dotted curves denote the $M_{WD} = 1.37 M_{\odot}$ model, but with a different chemical composition, $X_{C+O} = 0.4$ and 0.8 , respectively. Circles denote the starting points of light-curve fitting in Fig. 5; upper and lower points of $M_{WD} = 1.37 M_{\odot}$ (solid line) correspond to models 4 and 3, and those of $1.377 M_{\odot}$ (solid line) correspond to models 8 and 7, respectively (see Table 2). A short straight solid line indicates the decline rate of observed V data in Fig. 1 (3.3 mag/230 days).

V light curve in Figure 1. The length of the line indicates the observed period, which is relatively short because of dust blackout 230 days after the optical maximum. We cannot compare the entire evolution period of the light curve with the observational data, so fitting leaves some ambiguity in choosing the best-fit model, even though we may conclude that WDs with masses of $M_{WD} \lesssim 1.33 M_{\odot}$ are very unlikely because their light curves are too slow to be comparable with the observation.

Figure 5 represents the light-curve fitting with observational data. Here the model light curves of I_C are identical to those of V , but are shifted by 1.12 mag upward, the mean value of $V - I_C$ obtained in Figure 2. It should be noted that, in this figure, these light curves are further shifted by 1.0 mag because of $I_C - 1$.

These light curves are a part of the model light curves in Figure 4. In the early phase of the outburst, the light curve declines almost linearly, so that fitting is not unique. We can fit any part of our model light curve if its decline rate is the same as $\approx 0.014\text{--}0.015$ mag day $^{-1}$, for example, either the top or the middle part of the same light curve of the $1.377 M_{\odot}$ WD in Figure 4. In such a case, we show two possible extreme cases, i.e., the earliest starting point and the latest one, as shown in Figure 4 (circles). These model parameters are summarized in Table 2, where we distinguish the models by numbers.

Thus, we have selected several light curves that show a reasonable agreement with the observation. However, we cannot choose the best-fit model among them, because the observed period is too short to distinguish a particular light curve from others because the difference among them appears only in a late stage.

For relatively less massive WDs of $M_{WD} \lesssim 1.33 M_{\odot}$, we cannot make reasonable fits with the observation for any part of the model light curves. Among relatively more massive WDs of $M_{WD} \gtrsim 1.35 M_{\odot}$ in Table 2, model 1 shows a slightly slower decline. Therefore, the $1.35 M_{\odot}$ WD may be the lowest value for the WD mass. Thus, we may conclude that V445 Pup contains a very massive WD of $M_{WD} \gtrsim 1.35 M_{\odot}$.

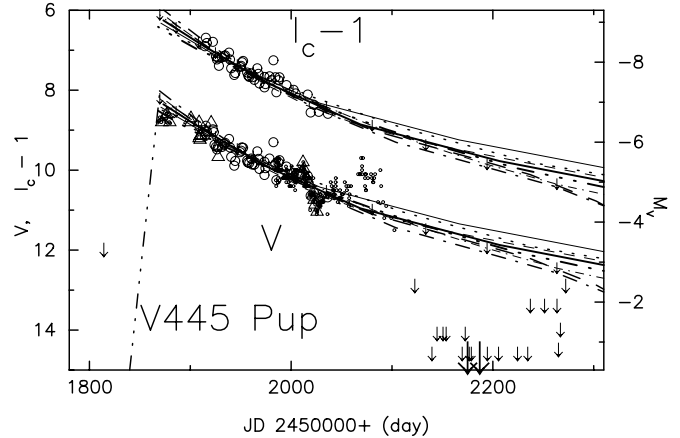


FIG. 5.—Our model light curves fitted to the observations. Dotted line, model 1; thin dashed line, model 2; thin solid line, model 3; thick solid line, model 4; triple-dot-dashed line, model 5; thin dash-dotted line, model 6; thick dashed line, model 7; dash-dotted line, model 8. Our model I_C light curves are identical to those of V , but are shifted up by 1.12 mag (and further shifted up by 1 mag for $I_C - 1$). The ordinate on the right vertical axis represents the absolute magnitude of model 4. For the other models, the model light curves are shifted down by 0.4 mag (model 1), up by 0.2 mag (model 2), up by 0.3 mag (models 3 and 7), down by 0.2 mag (model 5), down by 0.5 mag (model 6), and up by 0.1 mag (model 8) (see Table 2). The observational data are the same as those in Fig. 1.

3.3. Mass Accumulation Efficiency

During helium nova outbursts, part of the helium envelope is blown off by winds, while the rest accumulates on the WD. We define the mass accumulation efficiency η_{He} as the ratio of the envelope mass that remains on the WD after the helium nova outburst to the helium envelope mass at ignition, $\Delta M_{He,ig}$ (Kato & Hachisu 2004).

The mass accumulation efficiency is estimated as follows. We have calculated the mass lost by winds during the outburst, ΔM_{ej} . Note that ΔM_{ej} is the calculated total ejecta mass that is ejected during the wind phase, and not the mass ejected during the observing period, which may be shorter than the wind phase.

The ignition mass is approximated by the envelope mass at the optical peak, i.e., $\Delta M_{He,ig} \approx \Delta M_{He,peak}$. Since the exact time of the optical peak is unknown, we assume that the optical peak is reached on JD 2,451,872, i.e., the earliest prediscoversy observation in the brightest stage reported in IAU Circulars 7553, 28 days earlier than the discovery. The envelope mass at the optical peak is estimated from our wind solution and is listed as $\Delta M_{He,ig}$ in Table 2. The resultant accumulation efficiency,

$$\eta_{He} \equiv \frac{\Delta M_{He,peak} - \Delta M_{ej}}{\Delta M_{He,peak}}, \quad (3)$$

is also listed in Table 2. The efficiencies are as high as $\sim 50\%$. The WD of V445 Pup is already very massive ($M_{WD} \gtrsim 1.35 M_{\odot}$), and its mass has increased through helium nova outbursts. Therefore, V445 Pup is a strong candidate for a Type Ia supernova progenitor.

4. QUIESCENT PHASE

Before the 2000 outburst, there was a 14.5 mag star at the position of V445 Pup (taken from the archive of VSNET²), but no bright star has been observed since the dust blackout. We may regard 14.5 mag as the preoutburst magnitude of the binary.

² See <http://vsnet.kusastro.kyoto-u.ac.jp/vsnet>.

TABLE 2
PARAMETERS OF FITTED MODEL

Model No. (1)	M_{WD} (M_{\odot}) (2)	Y (3)	$X_{\text{C+O}}$ (4)	$\Delta M_{\text{He,ig}}^{\text{a}}$ (M_{\odot}) (5)	$\Delta M_{\text{ej}}^{\text{b}}$ (M_{\odot}) (6)	$\eta_{\text{He}}^{\text{c}}$ (7)	Distance (kpc) (8)	$\dot{M}_{\text{He}}^{\text{d}}$ ($M_{\odot} \text{ yr}^{-1}$) (9)	$\tau_{\text{rec}}^{\text{d}}$ (yr) (10)
1.....	1.35	0.38	0.6	3.3E-4	1.8E-4	0.45	6.6	6.E-8	5000
2.....	1.37	0.58	0.4	1.6E-4	9.2E-5	0.42	5.0	7.E-8	2000
3.....	1.37	0.38	0.6	1.9E-4	8.7E-5	0.53	4.8	6.E-8	3000
4.....	1.37	0.38	0.6	2.1E-4	1.1E-4	0.49	5.5	5.E-8	4000
5.....	1.37	0.18	0.8	3.5E-4	1.2E-4	0.64	6.0	4.E-8	9000
6.....	1.37	0.18	0.8	3.8E-4	1.5E-4	0.61	6.9	4.E-8	10000
7.....	1.377	0.38	0.6	1.8E-4	7.4E-5	0.60	4.8	5.E-8	4000
8.....	1.377	0.38	0.6	2.2E-4	9.6E-5	0.56	5.2	4.E-8	5000

^a Envelope mass at ignition is assumed to be equal to the mass at the optical peak, which we assume is JD 2,451,872 (28 days before the discovery).

^b Total mass ejected by the wind.

^c Mass accumulation efficiency.

^d Estimated from Fig. 7.

There are two possible explanations for this quiescent-phase luminosity; one is the accretion disk luminosity, and the other is the luminosity of the bright companion star. In the following subsections, we discuss how these possible sources contribute to the quiescent luminosity.

4.1. Accretion Disk

In some nova systems, an accretion disk mainly contributes to the brightness in their quiescent phase. If the preoutburst luminosity of V445 Pup comes from an accretion disk, its absolute magnitude is approximated by

$$M_V(\text{obs}) = -9.48 - \frac{5}{3} \log \left(\frac{M_{\text{WD}}}{M_{\odot}} \frac{\dot{M}_{\text{acc}}}{M_{\odot} \text{ yr}^{-1}} \right) - \frac{5}{2} \log (2 \cos i), \quad (4)$$

where M_{WD} is the WD mass, \dot{M}_{acc} the mass accretion rate, and i the inclination angle (eq. [A6] in Webbink et al. 1987). Assuming that $M_{\text{WD}} = 1.37 M_{\odot}$ and $i = 80^\circ$ (Woudt & Steeghs 2005), we have $M_V = 1.4, 2.3,$ and 3.1 for the accretion rates of $1 \times 10^{-6}, 3 \times 10^{-7},$ and $1 \times 10^{-7} M_{\odot} \text{ yr}^{-1}$, respectively.

The apparent magnitude of the disk is calculated from

$$m_V - M_V = A_V + 5 \log D_{10}, \quad (5)$$

where D_{10} is the distance divided by 10 pc. With the absorption of $A_V = 1.6$ and the distance of 3 kpc, the apparent magnitude is estimated to be $m_V = 15.4, 16.3,$ and 17.1 , for the above accretion rates, respectively. For the distance of 6.5 kpc, we obtain brightnesses of $m_V = 17.1, 18.0,$ and 18.8 , respectively. All of these values are much fainter than 14.5 mag. Therefore, it is very unlikely that an accretion disk mainly contributes to the preoutburst luminosity.

4.2. Helium Star Companion

Another possible source of the preoutburst brightness is a helium star companion. Figure 6 shows evolutionary tracks of helium stars with masses between 0.6 and $3.0 M_{\odot}$ from the helium main sequence to the red giant stage in the H-R diagram. We use OPAL opacities and an initial chemical composition of $X = 0.0, Y = 0.98,$ and $Z = 0.02$. The numerical method and input physics are the same as those in Saio (1995).

As shown in Figure 6, low-mass helium stars do not evolve to a red giant. In our new calculation, the $0.8 M_{\odot}$ helium star evolves to a red giant, but the 0.6 and $0.7 M_{\odot}$ helium stars evolve toward the blue. Paczyński (1971) showed that stars of $M_{\text{He}} \geq 1.0 M_{\odot}$ evolve to a red giant, while those with $0.5, 0.7,$ and $0.85 M_{\odot}$ do not. Our calculations are essentially the same as those of Paczyński (1971), and the difference is attributed mainly to the difference between the adopted opacities.

Figure 6 also shows locations of stars whose apparent magnitudes are $m_V = 14.5$ for $A_V = 1.6$. Here the distance is assumed to be 4.9 (*squares*) or 6.5 kpc (*circles*). For example, a star of (temperature, luminosity) = $(\log T_{\text{ph}}[\text{K}], \log L_{\text{ph}}/L_{\odot}) = (4.2, 2.81), (4.4, 3.25),$ and $(4.6, 3.75)$ could be observed as a 14.5 mag star for 6.5 kpc and $(\log T_{\text{ph}}[\text{K}], \log L_{\text{ph}}/L_{\odot}) = (4.2, 2.57), (4.2, 2.57), (4.4, 3.0),$ and $(4.6, 3.51)$ for 4.9 kpc.

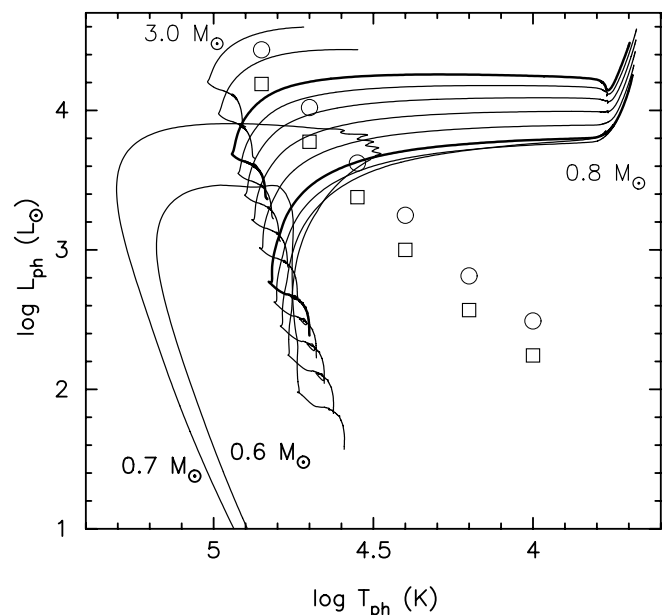


FIG. 6.— Evolutionary tracks of helium stars with masses of $M_{\text{He}} = 0.6, 0.7, 0.8, 0.9, 1.0$ (lower thick line), $1.2, 1.4, 1.6, 1.8, 2.0$ (upper thick line), $2.5,$ and $3.0 M_{\odot}$ in the H-R diagram. The 0.6 and $0.7 M_{\odot}$ stars evolve blueward and do not become red giants. We stopped the calculation when carbon ignites at the center for 2.5 and $3.0 M_{\odot}$ stars. Circles and squares denote stars with a 14.5 mag brightness at the distance of 6.5 and 4.9 kpc, respectively, for $A_V = 1.6$. [See the electronic edition of the Journal for a color version of this figure.]

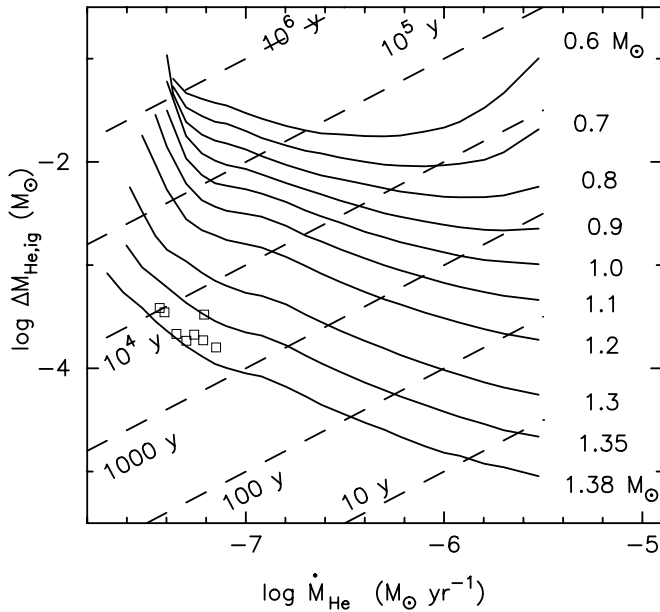


FIG. 7.—Helium ignition mass, $\Delta M_{\text{He,ig}}$, of helium-accreting WDs plotted against the helium accretion rate, \dot{M}_{He} . The WD mass is attached to each curve. Dashed lines indicate the recurrence period. Squares indicate the ignition mass of each model in Table 2. [See the electronic edition of the *Journal* for a color version of this figure.]

Therefore, the observed 14.5 mag is consistent with the luminosities and temperatures of slightly evolved helium stars of $M_{\text{He}} \gtrsim 0.8 M_{\odot}$ if the companion is a blue star of $\log T_{\text{ph}} \gtrsim 4.5$.

On the other hand, if the companion is redder than $\log T_{\text{ph}} \lesssim 4.4$, there is no corresponding evolution track in the low-luminosity region of the H-R diagram, as shown in Figure 6. In such a case, the preoutburst luminosity cannot be attributed to a helium star companion. T. Kato³ suggested that the preoutburst color of V445 Pup was much bluer than that of symbiotic stars (which have a red giant companion), but rather close to that of cataclysmic variables (main sequence or slightly evolved companion). This argument is consistent with our estimate of relatively high surface temperature $\log T_{\text{ph}} \gtrsim 4.5$ (see Fig. 6).

5. DISCUSSION

5.1. Distance

As explained in §§ 3.1 and 3.2, we do not solve for energy transfer outside the photosphere and, thus, we cannot determine the proportionality constant in equation (2). Therefore, we cannot determine the distance to V445 Pup directly by comparing the theoretical absolute magnitude with the observational apparent magnitude. Instead, we can estimate the approximate distance by assuming that the free-free flux is larger than the blackbody flux during the observing period. This assumption gives a lower limit to the distance. We expect that the distance thus estimated is close to the real value. Column (8) of Table 2 lists the distance estimated for each model. These distances are consistent with the observational estimates of $3.5 \text{ kpc} \lesssim d \lesssim 6.5 \text{ kpc}$ (Iijima & Nakanishi 2008) and $\sim 4.9 \text{ kpc}$ (Woudt & Steeghs 2005).

5.2. Helium Ignition Mass and Recurrence Period

We have calculated evolution of C+O white dwarfs accreting helium at various rates until ignition of a helium shell flash.

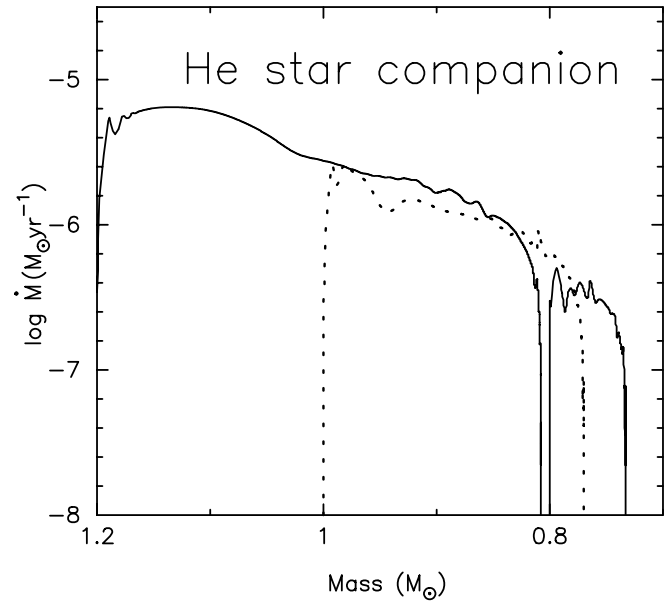


FIG. 8.—Mass-loss rate of a helium star that fills its Roche lobe of radius $1.5 R_{\odot}$. The initial stellar mass is 1.2, 1.0 (dotted line), and $0.8 M_{\odot}$. Time increases from left to right. See the text for more details.

Chemical compositions assumed are $X_{\text{C}} = 0.48$ and $X_{\text{O}} = 0.50$ for the WD core and $X = 0.0$ and $Y = 0.98$ for the accreted envelope. The initial model adopted for a given core mass and accretion rate is a steady state model in which the heating due to the accretion is balanced by the radiative energy flow. Adopting such an initial model is justified because the WD has accreted matter from the companion for a long time and experienced many shell flashes.

As the helium accretion proceeds, the temperature at the bottom of the envelope gradually increases. When the temperature becomes high enough, the triple-alpha reaction causes a shell flash. The mass of the helium envelope at ignition depends on the WD mass and the accretion rate, as shown in Figure 7. The envelope mass required to ignite a shell flash tends to be smaller for a higher accretion rate and for a larger WD mass. Helium flashes are weaker for higher accretion rates and lower WD masses. In particular, they are very weak for accretion rates higher than $\sim 10^{-6} M_{\odot} \text{ yr}^{-1}$.

The envelope mass at ignition depends also on the core temperature. If the core temperature of the initial WD is lower than that of the steady state model employed for our calculations, the envelope mass at ignition would be larger.

The recurrence period, $\Delta M_{\text{He,ig}}/\dot{M}_{\text{He}}$, is also plotted in Figure 7 by dashed lines. The recurrence periods corresponding to the ignition mass of our fitted models are listed in Table 2.

5.3. Mass Transfer from a Helium Star Companion

We have estimated the mean accretion rate \dot{M}_{He} of the WD as in Table 2. The companion star feeds its mass to the WD via the Roche lobe overflow or by winds, depending on whether it fills the Roche lobe or not. Here we examine whether this accretion rate is comparable to the mass transfer rates of the Roche lobe overflow from a helium star companion. We followed the stellar evolution of helium stars from the main sequence assuming that the star always fills its effective Roche lobe, for which the radius is simply assumed to be $1.5 R_{\odot}$. The resultant mass-loss rates are shown in Figure 8 for stars with initial masses of 1.2, 1.0 and $0.8 M_{\odot}$. These results are hardly affected, even if we change the Roche lobe radius.

³ See <http://www.kusastro.kyoto-u.ac.jp/vsnet/Mail/alert5000/msg00493.html>.

The mass-loss rate decreases with the companion mass almost independently of the initial value. Except for the short initial and final stages, these rates are as large as $M_{\text{He}} \sim 10^{-6} M_{\odot} \text{ yr}^{-1}$ and much larger than the mass accretion rate estimated from our fitted models in Table 2. Since almost all of the mass lost by the companion accretes onto the WD in the case of Roche lobe overflow, the accretion may result in very weak shell flashes for rates as high as $10^{-6} M_{\odot} \text{ yr}^{-1}$. A strong shell flash like V445 Pup is realized only in the final stages of mass transfer, when the mass transfer rate quickly drops with time. This rare case may correspond to a final stage of binary evolution after the WD has grown in mass to near the Chandrasekhar limit from a less massive one and the companion has lost a large amount of mass via Roche lobe overflow. Such information will be useful for modeling a new path of the binary evolution scenario that will lead to a Type Ia supernova.

5.4. Comparison with Other Observations

The mass of the dust shell can be estimated from infrared continuum flux with the assumption that the emission originated from warm dust. With infrared $10 \mu\text{m}$ spectrum, Lynch et al. (2004a) estimated the dust mass to be $2 \times 10^{-6} M_{\odot}$ for a distance of 3 kpc. This value would be increased if we adopt a larger distance instead of 3 kpc, but is still consistent with our estimated ejecta mass $\Delta M_{\text{ej}} \sim (0.7\text{--}1.8) \times 10^{-4} M_{\odot}$ in Table 2, because the dust mass is a small part of the ejected mass.

Lynch et al. (2004b) reported the absence of He II or coronal lines on their near-IR spectra and suggested that the ionizing source was not hot enough on 2004 January 14 and 16 (1146 days after the optical maximum). Lynch et al. (2005) also reported, from their near-IR observation on 2005 November 16, that the object had faded, and the thermal dust emission had virtually disappeared. They suggested that the dust had cooled significantly until that date (1818 days). This suggestion may constrain the WD mass of V445 Pup, because Figure 4 shows that the outburst lasts more than 1800 days for less massive WDs ($\lesssim 1.33 M_{\odot}$). If the WD had cooled down until the above date, we may exclude less massive WD models ($\lesssim 1.33 M_{\odot}$), because these WDs evolve slowly and their hot surfaces emit high-energy photons at least until 1800 days after the optical peak.

We have shown that the WD mass of V445 Pup is increasing with time. When the WD continues to grow to the Chandrasekhar limit, central carbon ignition triggers a Type Ia supernova explosion if the WD consists of carbon and oxygen. We regard the star as a CO WD instead of an O-Ne-Mg WD, because no indication of neon was observed in the nebula-phase spectrum (Woudt & Steeghs 2005). Therefore, we consider that V445 Pup is a strong candidate for a Type Ia supernova.

When a binary consisting of a massive WD and a helium star like V445 Pup becomes a Type Ia supernova, its spectrum may more or less show signs of helium. The search for such helium associated with a Type Ia supernova has been reported for a dozen Type Ia supernovae (Marion et al. 2003; Mattila et al. 2005), but all of them are null detections. It may be difficult to find such a system, because this type of Type Ia supernova is very rare.

The binary seems to be still deeply obscured by the optically thick dust shell, even several years after the outburst. This blackout period is much longer than that of the classical novae, such as OS And (~ 20 days), V705 Cas (~ 100 days), and DQ Her (~ 100 days). As the ejected mass estimated in Table 2 is not much different from those of classical novae, the difference in the blackout period may be attributed to a large amount of dust in the extremely carbon-rich ejecta of a helium nova. Moreover, the observed low ejection velocities of $\sim 500 \text{ km s}^{-1}$ (Iijima & Nakanishi 2008) are not much larger than the escape velocity of the binary with a relatively large total mass [e.g., $1.35 M_{\odot} + (1\text{--}2) M_{\odot}$]. Both of these effects lengthen the dust blackout period. When the dust obscuration is cleared in the future, the period of blackout will provide useful information about the dust shell.

6. CONCLUSIONS

Our main results are summarized as follows:

1. We have reproduced V and I_C light curves using free-free emission-dominated light curves calculated on the basis of the optically thick wind theory.
2. From the light-curve analysis, we have estimated the WD mass to be as massive as $M_{\text{WD}} \gtrsim 1.35 M_{\odot}$.
3. Our light-curve models are now consistent with a longer distance of $3.5 \text{ kpc} \lesssim d \lesssim 6.5 \text{ kpc}$ (Iijima & Nakanishi 2008) and 4.9 kpc (Woudt & Steeghs 2005).
4. We have estimated the ejecta mass as the mass lost by optically thick winds, i.e., $\Delta M_{\text{wind}} \sim 10^{-4} M_{\odot}$. This amounts to about half of the accreted helium matter so that the accumulation efficiency reaches $\sim 50\%$.
5. The white dwarf is already very close to the Chandrasekhar mass, i.e., $M_{\text{WD}} \gtrsim 1.35 M_{\odot}$, and the WD mass had increased after the helium nova. Therefore, V445 Pup is a strong candidate for a Type Ia supernova progenitor.
6. We emphasize the importance of making observations after the dense dust shell disappears, especially observations of the color and magnitude, orbital period, and inclination angle of the orbit. These are important to specify the nature of the companion.

M. K. and I. H. are grateful to people at the Astronomical Observatory of Padova and at the Department of Astronomy of the University of Padova, Italy, for their warm hospitality. Especially we thank Takashi Iijima for fruitful discussions on V445 Pup, which inspired us to start this work. The authors thank Masaomi Tanaka for information on the helium detection in Type Ia supernovae. We also thank the anonymous referee for useful comments that improved the manuscript. Thanks are also due to the American Association of Variable Star Observers (AAVSO) for the photometric data of V445 Pup and Taichi Kato for introducing us to the discussion in VSNET. This research has been supported in part by the Grants-in-Aid for Scientific Research (16540211, 20540227) from the Japan Society for the Promotion of Science.

REFERENCES

- Ashok, N. M., & Banerjee, D. P. K. 2003, *A&A*, 409, 1007
 Black, J. H., & Gallagher, J. S. 1976, *Nature*, 261, 296
 Brown, R. L., & Mathews, W. G. 1970, *ApJ*, 160, 939
 Ferland, G. J. 1977, *ApJ*, 215, 873
 Gallagher, J. S., & Ney, E. P. 1976, *ApJ*, 204, L35
 Hachisu, I., & Kato, M. 2003, *ApJ*, 590, 445
 ———. 2006, *ApJS*, 167, 59
 ———. 2007, *ApJ*, 662, 552
 Hachisu, I., Kato, M., & Cassatella, A. 2008, *ApJ*, in press (arXiv:0806.4253)
 Hachisu, I., Kato, M., Kato, T., & Matsumoto, K. 2000, *ApJ*, 528, L97
 Hachisu, I., Kato, M., & Luna, G. J. M. 2007, *ApJ*, 659, L153
 Hachisu, I., Kato, M., & Nomoto, K. 1999a, *ApJ*, 522, 487
 Henden, A. A., Wagner, R. M., & Starrfield, S. G. 2001, *IAU Circ.* 7730
 Iglesias, C. A., & Rogers, F. J. 1996, *ApJ*, 464, 943
 Iijima, T., & Nakanishi, H. 2008, *A&A*, 482, 865
 Kamath, U. S., & Anupama, G. C. 2002, *Bull. Astron. Soc. India*, 30, 679

- Kato, M., & Hachisu, I. 1994, *ApJ*, 437, 802
———. 1999, *ApJ*, 513, L41
———. 2003, *ApJ*, 598, L107
———. 2004, *ApJ*, 613, L129
- Kato, M., Saio, H., & Hachisu, I. 1989, *ApJ*, 340, 509
- Kato, T., Kanatsu, K., Takamizawa, K., Takao, A., & Stubbings, R. 2000, *IAU Circ.* 7552
- Kolotilov, E. A., & Liberman, A. A. 1976, *Soviet Astron. Lett.*, 2, 37
- Lynch, D. K., Rudy, R. J., Mazuk, S., & Venturini, C. C. 2004a, *AJ*, 128, 2962
- Lynch, D. K., Rudy, R. J., Mazuk, S., Venturini, C. C., Puetter, R. C., & Perry, R. B. 2004b, *IAU Circ.* 8278
- Lynch, D. K., Rudy, R. J., Venturini, C. C., Mazuk, S., Puetter, R. C., Perry, R. B., & Walp, B. 2005, *IAU Circ.* 8642
- Marion, G. H., Höflich, P., Vacca, W. D., & Wheeler, J. C. 2003, *ApJ*, 591, 316
- Mattila, S., Lundqvist, P., Sollerman, J., Kozma, C., Baron, E., Fransson, C., Leibundgut, B., & Nomoto, K. 2005, *A&A*, 443, 649
- McGowan, K. E., Charles, P. A., Blustin, A. J., Livio, M., O'Donoghue, D., & Heathcote, B. 2005, *MNRAS*, 364, 462
- Nomoto, K., Thielemann, F., & Yokoi, K. 1984, *ApJ*, 286, 644
- Paczyński, B. 1971, *Acta. Astron.*, 21, 1
- Saio, H. 1995, *MNRAS*, 277, 1393
- Schmidtke, P. C., & Cowley, A. P. 2006, *AJ*, 131, 600
- Shenavrin, V. I., & Moroz, V. I. 1976, *Soviet Astron. Lett.*, 2, 39
- Webbink, R. F., Livio, M., Truran, J. W., & Orio, M. 1987, *ApJ*, 314, 653
- Woudt, P. A. 2002, *IAU Circ.* 7955
- Woudt, P. A., & Steeghs, D. 2005, in *ASP Conf. Ser.* 330, *The Astrophysics of Cataclysmic Variables and Related Objects*, ed. J. M. Hameury & J. P. Lasota (San Francisco: ASP), 451